Effect of Strain Hardening on the Flexural and Compressive Properties of Fiber Reinforced Clay-Matrix Composite

Group 4

Team Members:

Kofi Sannie Amosah - 34342024

Latifa Abdul-Manaf - 28612024

Asher Chakupa - 49952024

Yamoah Frimpong Attafuah - 58222024

Lecturer: Dr. Danyuo Yiporo

SC221: Material Science and Chemistry

Cohort B

Date: 9th December 2022

1.0 Introduction

Humans have used composite materials for thousands of years. Consider mud bricks as an example. A cake of dried mud will crumble when you attempt to bend it, but if you crush or compress it, it will hold its shape. Contrarily, a straw has considerable strength when stretched but nearly none when compressed. The qualities of these two materials are combined when mud and straw are used to make a block, giving you a brick that is resistant to bending, tearing, and compression. Composite materials are formed by combining two or more physically identifiable materials with different properties. The other materials work together to give unique composite properties. Still, within the composite, you can quickly tell the different materials apart – they do not dissolve or blend into each other (Curious, 2017).

The various components of a composite serve as either the reinforcement or the matrix. The matrix surrounds and binds together a cluster of fibers or fragments of material with different properties – the reinforcement. FRC is a high-performance fiber composite achieved and made possible by cross-linking cellulosic fiber molecules with resins in the FRC material matrix through a proprietary molecular re-engineering process, yielding a product of exceptional structural properties (Park & Seo, 2011). Aerospace systems and automotive, industrial, and consumer goods continue to utilize fiber-reinforced composite materials. Fiber-reinforced composite materials are being created and employed in numerous additional situations to replace metal components, especially those used in corrosive conditions. Due to their growing use in structural applications, the nondestructive evaluation of fiber-reinforced composites continues to garner much interest in research and development (Park & Seo, 2011).

This experiment employed clay bricks as a case study for our experiment and broadly examined their composition. We could ascertain how the matrix-fiber composition affects the properties of composite materials by creating composites of clay and fiber with various compositions, as shown by compression and three-point bend tests carried out on the multiple samples. To identify which set of bricks had the best qualities, we conducted tests using the PASCO testing apparatus. The team developed samples with the same dimensions but varied compositions to make it easier to compare the investigated properties. We tried constructing the bricks multiple times during the creation stage before learning to shape them into nearly perfect cuboids that could be utilized as suitable test samples. Obtaining an excellent clay powder and combining it with the proper amounts of water and fiber to make our bricks was the first step in the brick-making process. Before doing hard work, we had to knead the clay and let it sit for a while.

The nearly perfect samples were essential because internal tensions or voids in the bricks would have affected our findings.

2.0 Materials and Methodology

2.1 Apparatus Used

- Clay ores
- Fiber
- Water
- PVC pipes
- Plywood
- Wooden roller
- Industrial woodcutter
- 1500 cm^3 beaker
- PASCO Comprehensive Materials Testing Machine
- Vernier calipers
- Hacksaw
- Scissors
- Sieves
- Computer
- Nails

2.2 Hypothesis

The addition of fibre as a reinforcing phase in clay produces a composite with improved compressive and flexural strength and toughness over pure clay.

2.3 Methodology

2.3.1 Sample Preparation

Clay ore was dried, pulverized, ground, and rolled into fine particles using a flat wooden block and board. It was then sieved twice and stored for two days, as shown in **Figures 9** and **20** of **Appendix B**. Rectangular molds were then constructed using plywood and an industrial cutter. First, 12 rectangular molds of length 7cm, width 2.5cm, and thickness 3cm were built, and next, 12 cylindrical molds of length 7cm and inner diameter 3cm were made using PVC pipes and a hacksaw, displayed in **Figures 17** and **19**. The now fine clay was mixed with a small amount of water and, via rolling and kneading, coldworked by hand and with a wooden roller. The specimens were stored for two days, after which the coldworking process was repeated until the samples became sticky and plastic. Two clay-fiber configurations were then produced, with clay as the matrix and fiber (shown in **Figure 10**) as the reinforcement, in volume ratios

of 100-0 and 50-50, in parts of 1200 cm^3 each, i.e., 1200 cm^3 of clay was mixed with 1200 cm^3 of fiber for the 50-50 ratio. These mixtures were kneaded and churned thoroughly to ensure the samples were as homogenous as possible. Both configurations were then compacted into rectangular and cylindrical molds, with five cylindrical samples and five rectangular samples for each configuration. These were stored in the molds and left to dry for three days. Images of the final samples can be found in **Figures 11-16**.

2.3.2 Mechanical Properties Investigation

After drying, the samples were removed from the molds, and their dimensions were measured, with the recorded values shown in **Tables 1** and **2** of **Appendix A**. The percentage shrinkage of the different samples was then calculated according to the formula:

$$Percentage\ Shrinkage = \frac{Initial\ Volume - Final\ Volume}{Initial\ Volume} \times 100\%,$$

Initial Volume is calculated from the mould dimensions, and Final Volume is calculated from the final measured dimensions of the dried specimen. This data is presented in **Tables 1** and **2**.

Using the Comprehensive Materials Testing Machine, shown in **Figure 18**, a compressive stress test was performed on the cylindrical samples of both the pure (100-0) composite and reinforced (50-50) composite to determine their compressive strengths by placing the cylinders in the vices of the machine and slowly rotating the hand crank clockwise until the composite was completely crushed. The compressive stress is calculated from the formula:

$$\sigma = \frac{F}{A}$$

Where *F* is Force, and *A* is the cross-sectional area of the cylindrical samples calculated from the formula:

$$A = \frac{\pi \times d^2}{4}$$

Where *d* is the diameter of the cylindrical samples.

The strain was calculated using the formula:

$$\epsilon = \frac{l_0 - l_f}{l_0}$$

where l_0 is the initial length of the cylindrical Sample and l_f is the final length of the samples.

Furthermore, using the Comprehensive Materials Testing Machine, a 3-point bend test was performed on the rectangular samples to determine their strengths, peak load, and flexural modulus. The flexural stress and strain of the samples were calculated according to the formulae:

$$\sigma_f = \frac{3\,FL}{2\,bd^2} \qquad \varepsilon_f = \frac{6\,dD}{L^2}$$

where σ_f is the flexural stress, ϵ_f is the flexural strain, F is the force applied, L is the distance between the two supports of the 3-point bend test, and b and d are the width and depth of the rectangular blocks, respectively. The flexural moduli were obtained from the slope of the linear region of the plotted stress-strain curves of the rectangular samples.

2.4 Precautions

- In using the PASCO Comprehensive Materials Testing Machine, the hand crank was rotated with a slow constant force.
- Gloves were used in the coldworking process to avoid blisters.
- The appropriate safety gear such as goggles were gloves were employed in the operation of the industrial cutter to cut plywood.

3.0 Results

3.1 Optical Observation using USB Microscope (Before Tests) (Appendix A: Fig. 1-4)

From the optical results, we can observe that the fiber-reinforced samples have fibers located within them and these fibers entangle with themselves and the matrix. It can also be observed that these fibers have been randomly arranged in different orientations and have different lengths.

3.2 Percentage Shrinkage Results. (Appendix A: Graph 1)

According to the graph, it can be observed that all samples attained an amount of percentage shrinkage. This can result from the cold work, so after drying, these samples shrank due to water loss. It can also be seen that the purest samples attained the highest percentage of

shrinkage. This is because of fibers in the reinforced samples, which act as interstitial structures which take up space and do not shrink.

3.3 Flexural Stress Strain for Samples. (Appendix: A Graph 2 and 3)

According to the Flexural Stress-Strain graph, it can be observed that all samples follow a similar trend of slowly increasing flexural stress and then maintaining a constant stress value throughout an array of strain values. This shows some toughness in the samples, meaning these samples can absorb a high amount of impact. According to the graph, the Flexural Stress-Strain curve of the pure samples rises overall to a peak and then collapses. This is because fracturing occurs at the maximum stress.

3.4 Flexural Moduli (Appendix A: Graph 4)

According to the data, the pure samples exhibit a higher Flexural modulus because cold working increases, increasing the dislocation densities in the samples. Also, because they are hard and brittle, they quickly broke earlier in the test compared to the fiber-reinforced samples.

3.5 Average Flexural Stress-Strain (Appendix A: Graph 5)

It can be observed that the fiber-reinforced materials reach a higher stress peak than the pure ones. Also, the fiber-reinforced samples show a trend of toughness, whiles the pure samples show a trend of hardness and brittleness; therefore, they experienced earlier fracturing.

3.6 Compressive Tests Results (Appendix A: Graph 6)

The compressive test results show that although the pure samples could take a higher compressive load, they were easily fractured. However, the fiber-reinforced samples strained and showed a trend of toughness.

3.7 Optical Observation using USB Microscope (After Tests) (Appendix: A Fig. 5-8)

The fibers in the reinforced samples can be seen from the USB optical images after the tests were conducted. Due to the 50-50 percent ratio, it can be observed that a lot of fibers are visible. For the pure samples, grains containing different sizes of sand and quartz particles of different sizes and colors can be observed.

The fibers in the reinforced samples can be seen from the USB optical images after the tests were conducted. Due to the 50-50 percent ratio, it can be observed that a lot of fibers are visible.

For the pure samples, grains containing different sizes of sand and quartz particles of different sizes and colors can be observed.

4.0 Discussion

After drying the reinforced and pure samples, shrinkage was observed on the samples due to the water's evaporation that constituted the matrix's volume. As shown in ***Graph 1***, the reinforced samples having a smaller volume of clay than the pure Sample resulted in a minor shrinkage since the reinforcement fiber sucked a small volume of water compared to the volume it occupied in the matrix. Hence, the matrix volume holding water was smaller than the control sample. However, slow drying made the clay more compact, and fewer cracks were observed as the water evaporated slowly from the samples.

The microstructure of pure and reinforced samples sparked a hypothesis of what to expect after the tests, which aligned with the results. From both ***Figure 1*** and ***Figure 2***, the reinforcement fibers and the matrix are loosely bonded, and the degree of compactness is lower compared to the pure samples illustrated in ***Figure 3*** and ***Figure 4***, which show a high level of compactness on the grains. The high level of compactness of grains on the pure Sample in ***Figure 3*** and ***Figure 4*** depicts an increase in yield strength and strain hardening coefficient, which the Hall-Petch equation and Ludwik's equation explain well below.

$$\sigma_y = \sigma_0 + \frac{k_y}{\sqrt{d}} \qquad \bar{\sigma} = \sigma_y + K\bar{\varepsilon_p}^n$$

Where σ_y is the yield strength, K and k_y are constant s, σ_o is the original yield stress, n is the strain hardening constant and ε_p is the true strain.

The increase in the amount of cold work decreases the magnitude of d, the average grain diameter, thus increasing the magnitude of yield strength. On the other hand, the magnitude of ε is directly proportional to the yield strength.

The grain size was reduced, and dislocation pile-up and twinning occurred extensively due to cold working. The number of dislocations within a grain affects the stress build-up in the adjacent grain, which activates dislocation sources and enables deformation in both grains. However, grain boundaries are an impassable barrier for dislocations. Yield strength and dislocation accumulation at grain boundaries were both affected by grain size. Altogether, this accounts for the flexural modulus visualized from the ***Graph*** 4, which contrasts the pure

samples and reinforced samples, which means that the pure samples are brittle and tougher than the reinforced samples.

In the account of the flexural stress-strain of the two samples, the reinforced Sample topped in the ultimate yield strength compared to the pure Sample due to the high modulus of elasticity of the fibers. Furthermore, the large area under ***Graph 5***, the reinforced flexural stress-strain graph signifies high toughness, enhanced by the fiber reinforcements to the matrix. On the other hand, low toughness is depicted from the pure Sample.

Random alignment of fibers in the matrix gave a higher strength in the longitudinal axis, as illustrated by ***Graph 6***, and the flexural stress-strain graph shows lateral weakness. A conclusion can be drawn that the randomness was skewed, favoring the longitudinal arrangement, thus, more strength in the longitudinal axis.

We propose that in the future, standard low-cost chemical stabilizers such as cement and lime be added to clay in order to achieve maximum compactness and the desired results of minimizing shrinking while simultaneously increasing the material's tensile strength. Also, the three-dimensional arrangement of fiber reinforcement to enhance strength in all directions.

5.0 Conclusion

The team gained a deeper understanding of composite materials' qualities by examining the differences in mechanical properties between clay-fiber bricks and pure clay bricks. First, the results of the tests for compressive and flexural strength showed that fiber composite materials are significantly more durable than their homogeneous equivalent. The compressive and flexural strength graphs are accurate, with the 50-50%wt fiber composite bricks showing stronger ultimate compressive and flexural strength and greater strength under increasing strain. This validates our hypothesis: "the addition of fiber as a reinforcing phase in clay produces a composite with improved compressive and flexural strength and toughness over pure clay."

In contrast, pure clay bricks experienced brittle fractures when the maximum compressive or flexural strength was reached. Adding natural fibers enhances the mechanical behavior of various matrices' composites. Even though the acquired strengths are often lower than those of pure paste, which behaves in a fragile manner, the addition of the matrix's fibers ensures ductile behavior in both bending and compression.

The building industry has recently been characterized by a need to lessen the environmental impact of the materials utilized. To accomplish this, the selection of materials should consider sustainable development. In this context, building supplies with steel as their primary reinforcement vegetable fibers are increasingly receiving more attention due to the strong motivation from weight increase and solid mechanical attributes.

Plant fibers can replace synthetic fibers because they degrade quickly, are renewable, and provide intriguing, unique mechanical properties. With these, fibers are likely to be interested in sustainable development, giving additional advantages such as enhanced tensile strength and crack prevention can increase the materials' ductility (Belkhir & Merzoud, 2021).

Throughout the experiment, we encountered specific challenges; however, we did our best to achieve the best results. So much time was wasted on sieving the dry clay over and over to obtain very fine clay powder. Also, a lot of manpower went into the kneading of the clay; even more, energy was required to knead the clay when it was mixed with fiber. Aside from these challenges, we made some suggestions we could work on to improve the accuracy of our experiment in the future; it was noticed that adding fibers in different orientations and lengths would contribute to the improvement of results. Again, the inclusion of more ratios, such as 60-40 and 70-30 fiber-to-clay ratios, may help find the optimum composite arrangement. Lastly, testing with different types of reinforcements would provide a chance for a better comparison of results and, consequently, the accuracy of work.

Appendix A

Table 1: *Dimensions of rectangular block samples with percentage shrinkages*

	Pure Block			Fiber Block		
	1	2	3	1	2	3
Length (cm)	6.6	6.55	6.6	6.5	6.6	6.6
Width (cm)	2.8	2.6	2.6	2.7	2.6	2.7
Depth (cm)	2.3	2.4	2.1	2.3	2.4	2.2
Final Volume (cm3)	42.504	40.872	36.036	40.365	41.184	39.204
Initial Volume	52.5	52.5	52.5	52.5	52.5	52.5
Percent Shrinkage	19.04	22.14857	31.36	23.11429	21.55429	25.3257

Table 2: *Dimensions of cylindrical block samples with percentage shrinkages*

	Pure Cylinder			Fiber Cylinder		
	1	2	3	1	2	3
Length (cm)	6.4	6.5	6.5	6.7	7	6.8
Diameter (mm)	2.7	2.8	2.8	2.7	2.9	
Final Volume (cm3)	36.64350576	40.0238566	40.0238566	38.36117009	46.23635083	0
Initial Volume	49.4800425	49.4800425	49.4800425	49.4800425	49.4800425	49.48
Percentage Shrinkage	25.94285714	22.14857	31.36	23.11429	21.554286	25.3257

Figure 1: *USB image of the reinforced brick sample before testing.*

Figure 2: *USB image of the cylindrical reinforced sample before testing.*

Figure 3: *USB image of the pure brick sample before testing.*

Figure 4: *USB image of the cylindrical pure sample before testing.*

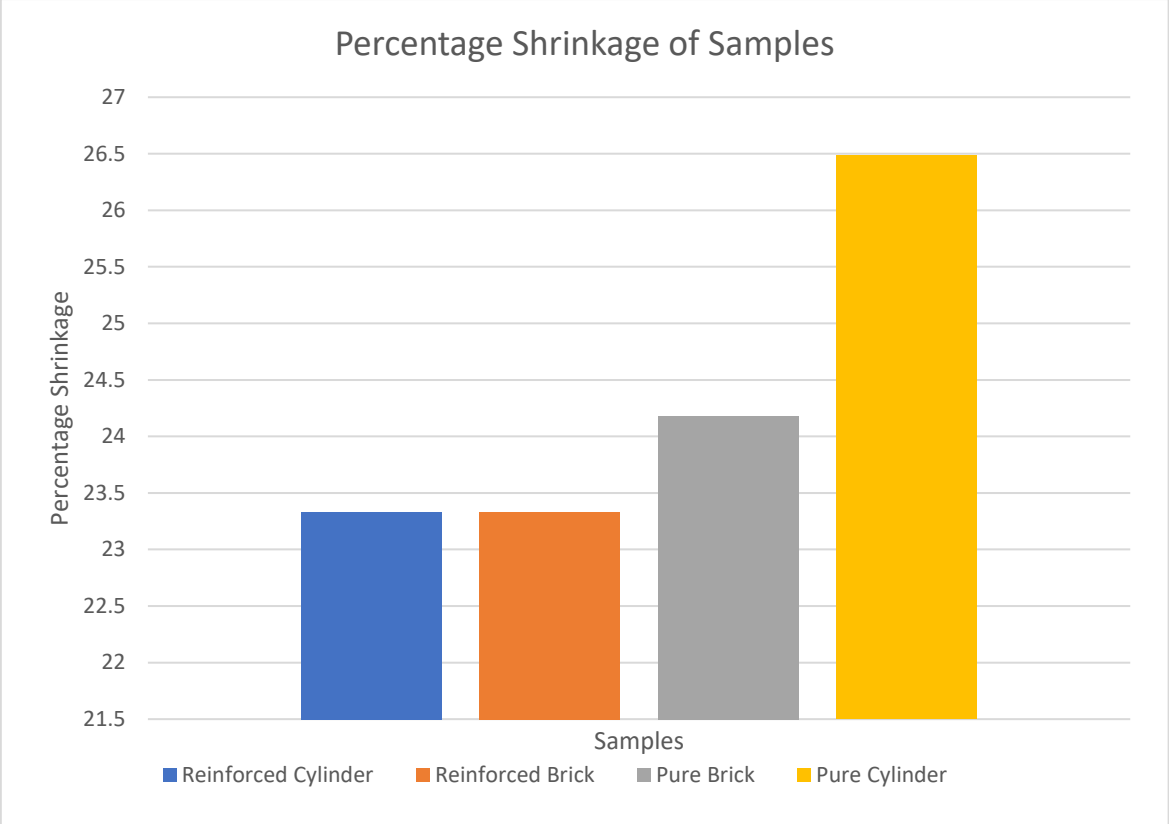

Graph 1: *Percentage Shrinkage of reinforced samples with pure clay samples*

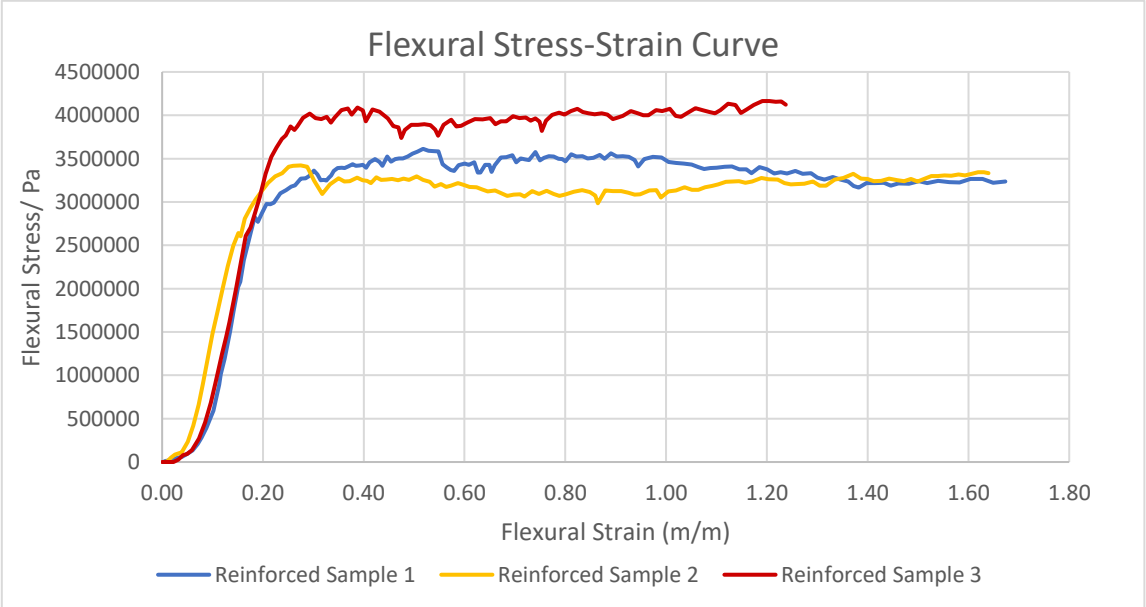

Graph 2: *Flexural Stress-Strain Curve for reinforced brick samples*

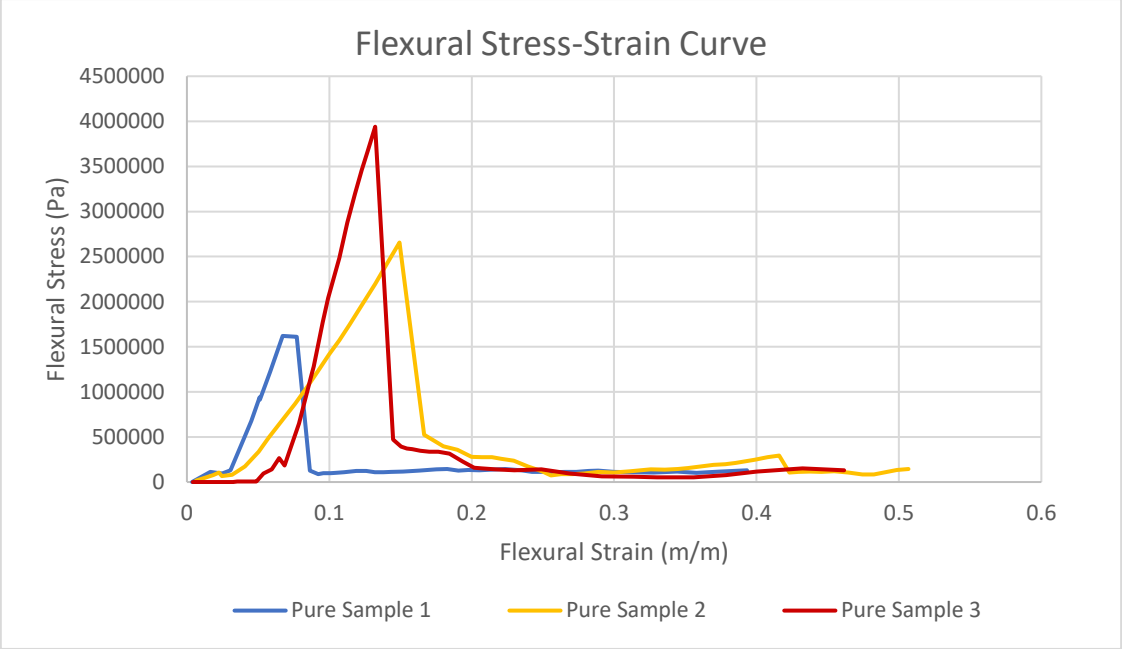

Graph 3: *Flexural Stress-Strain Curve for Pure brick samples*

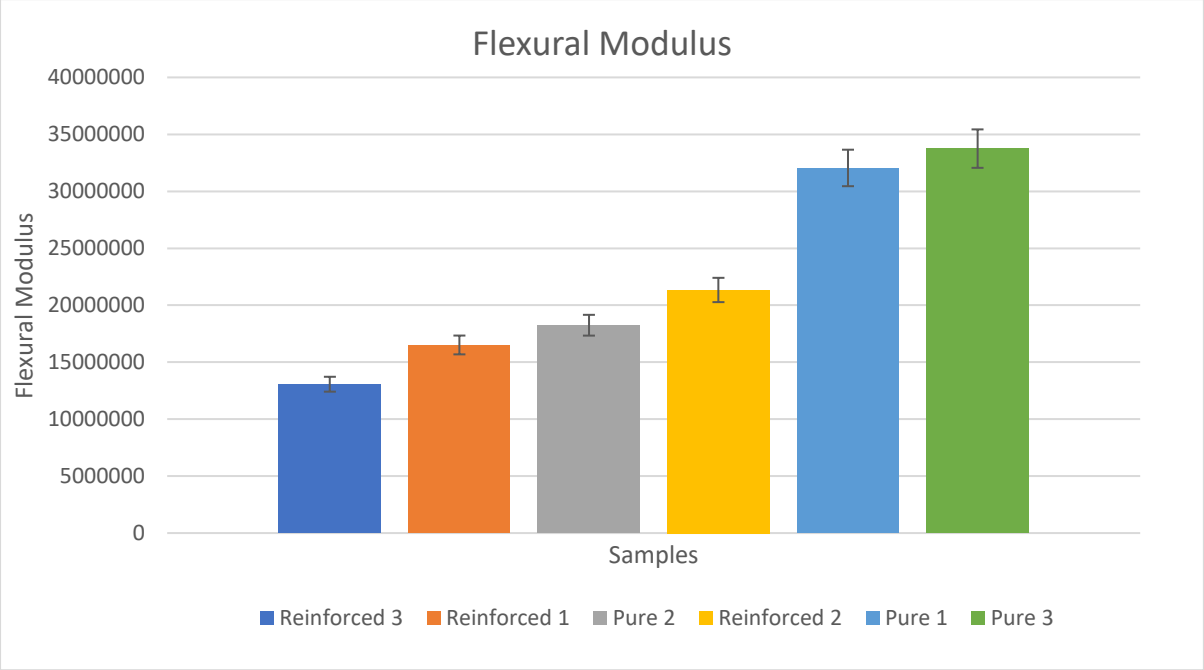

Graph 4: *Flexural Modulus for Pure brick samples*

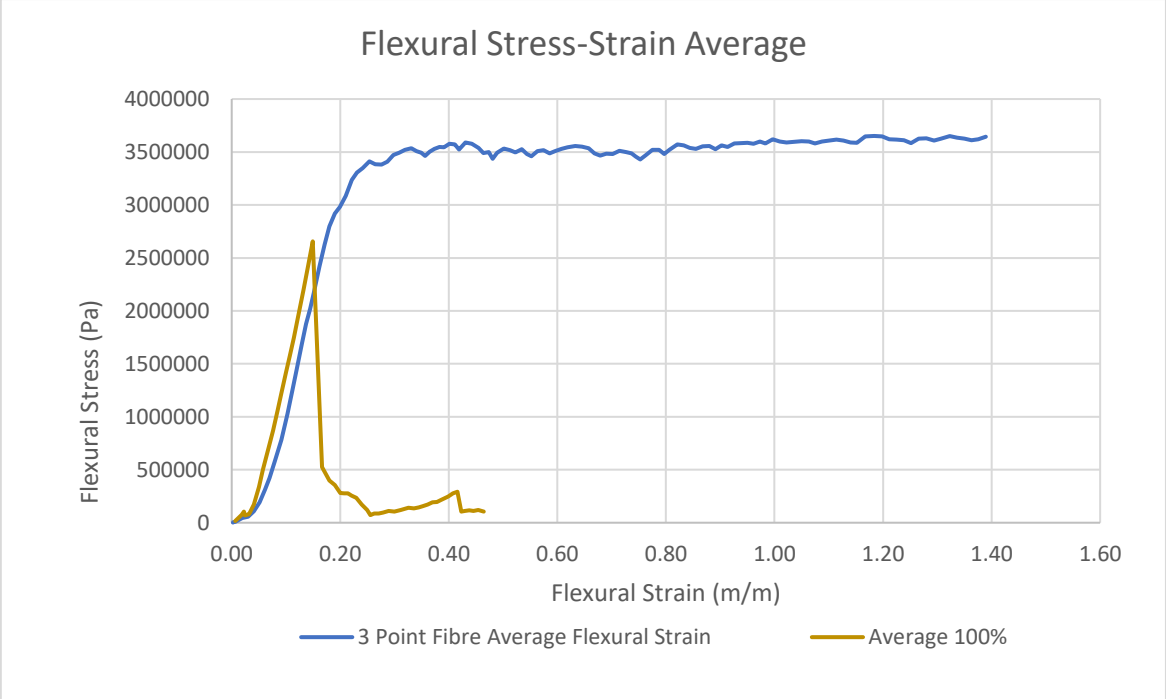

Graph 5: *Comparison of Average Flexural Stress-Strain Curve for brick samples*

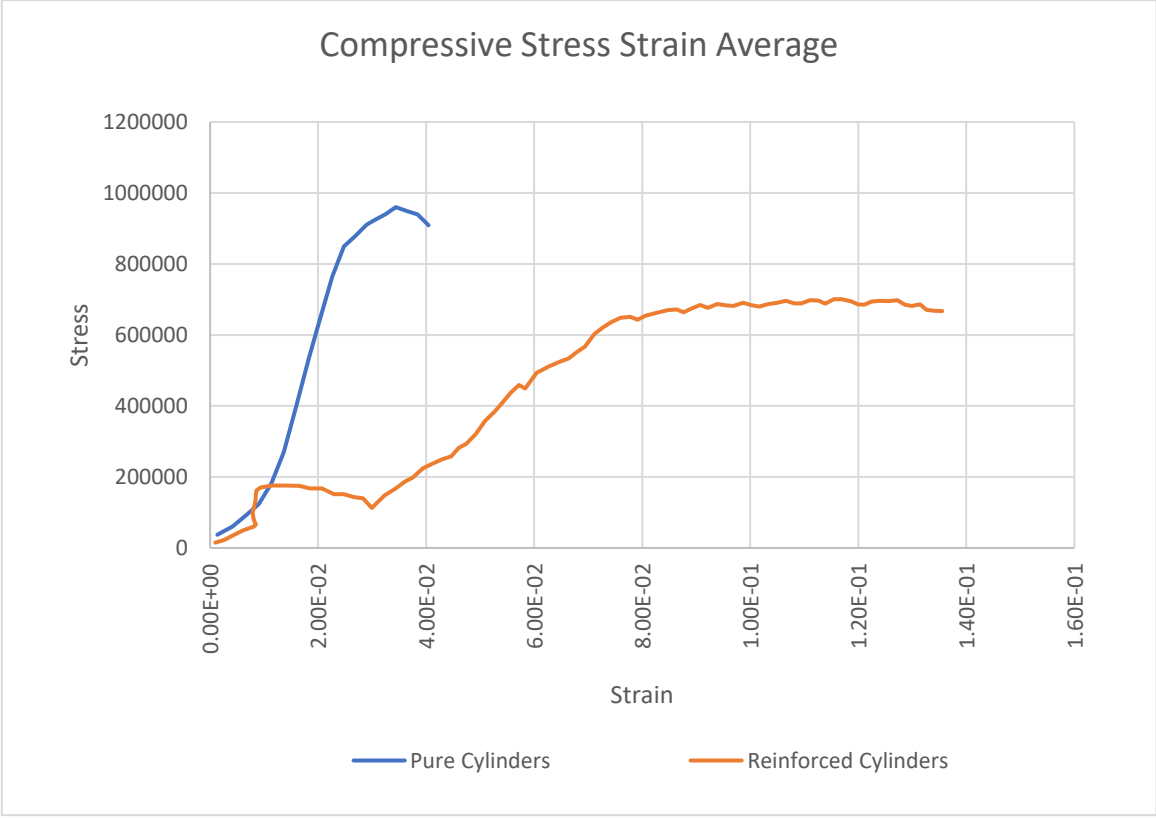

Graph 6: *Comparison of Average Compressive Stress-Strain Curve for cylindrical samples*

Figure 5: *USB image of fractured reinforced brick samples after the Test*

Figure 6: *USB image of fractured cylindrical reinforced samples after the Test*

Figure 7: *USB image of fractured pure brick samples after the Test*

Figure 8: *USB image of fractured cylindrical pure samples after the Test*

Appendix B

Figure 9: *Clay ore*

Figure 10: *Fibre*

Figure 11: *Pure Rectangular Samples*

Figure 12: *Reinforced Rectangular Samples*

Figure 13: *Reinforced Cylindrical Samples*

Figure 14: *Pure Cylindrical Samples*

Figure 15: *Samples produced excluding a pure cylindrical sample*

Figure 16: *Pure Rectangular Samples*

Figure 17: *Wooden rectangular moulds*

Figure 18: *PASCO Comprehensive Materials Testing Machine*

Figure 19: *PVC Cylindrical Mould*

Figure 20: *Group 4 members grinding and sieving the clay ore*

References

Curious. (2017, September 26). *The science and technology of composite materials*. Curious. https://www.science.org.au/curious/technology-future/composite-materials

Fibre-Reinforced Composite - an overview | ScienceDirect Topics. (n.d.). Www.sciencedirect.com. https://www.sciencedirect.com/topics/engineering/fibre-reinforced-composite

Interface Science and Technology | Book series | ScienceDirect.com. (2019). Sciencedirect.com. https://www.sciencedirect.com/bookseries/interface-science-and-technology

Belkhir, Z., & Merzoud, M. (2021). Improvement of the Mechanical Behavior of Composite Materials with Different Binders Based on Local Plant Fibers Alfa and Diss. *Civil and Environmental Engineering Reports*, *31*(4), 130–147. https://doi.org/10.2478/ceer-2021-0053

Park, S.-J., & Seo, M.-K. (2011, January 1). *Chapter 8 - Composite Characterization* (S.-J. Park & M.-K. Seo, Eds.). ScienceDirect; Elsevier. https://www.sciencedirect.com/science/article/abs/pii/B9780123750495000086